SimBuild 2006
Second National IBPSA-USA Conference
Cambridge, MA
August 2-4, 2006

THE SIMULATION OF A RENEWABLE-ENERGY-POWERED HYDROGEN-BASED RESIDENTIAL ELECTRICITY SYSTEM

Ian Beausoleil-Morrison, Maria Mottillo, Alex Ferguson, Hajo Ribberink, Libing Yang, and Kamel Haddad
CANMET Energy Technology Centre, Natural Resources Canada, Ottawa Canada

ABSTRACT

The integration of photovoltaics within buildings to meet local electricity demands offers great potential for reducing the environmental impact of central electricity production and distribution. However, the inherent temporal mismatch between electrical production and consumption represents a significant obstacle in the long-term. With the present low fraction of non-dispatchable power on most electrical distribution systems, it is technically feasible to use the grid to absorb excess power and to supply power during deficits of production. In the future, however, it is likely that some form of local storage will be required to reduce grid reliance. This paper examines a concept based upon the local production, storage, and conversion of hydrogen that might address that need. Models of the appropriate resolution are described and their calibration using empirical data discussed. The operation of these models is demonstrated and plans outlined for the use of the models to assess the feasibility of the concept.

INTRODUCTION

Renewable energy sources offer great potential for reducing the greenhouse gas (GHG) emissions and other environmental impacts of electricity production. Solar photovoltaics (PV), for example, can not only displace central fossil-fuel sources, they can also be implemented in a distributed fashion whereby electricity production and consumption are co-located. However, many technical challenges impede the widespread adoption of building-integrated PV (BIPV). A significant obstacle is the inherent temporal mismatch between electrical production and consumption. PV systems produce electricity when solar energy is available while buildings demand electricity in a semi-chaotic pattern that is highly dependent upon occupant behaviour.

Two techniques are commonly employed to address the inherent temporal mismatch between production and consumption. With off-grid buildings the common approach is to use battery storage to buffer between production and demand (and to level demand using load management techniques). Whereas with grid-connected buildings it is common to use the electrical network as a form of electrical storage, exporting to the grid when there is excess production and importing from the grid when production is insufficient. The former approach is impractical for storing large quantities of energy for moderate periods of time. And it is unlikely that the latter approach could be used should BIPV and other distributed renewable sources become a significant portion of the generation mix (10-20%), as such a large fraction of non-dispatchable power would create an unmanageable scenario for the network operator who must constantly balance supply and demand on the entire network.

A number of researchers have proposed a third alternative for buffering between production and consumption. With this, hydrogen (H_2) is produced locally by electrolysis at times of excess electrical production. H_2, acting as an energy carrier, is stored in pressurized containers and reconverted to electricity—either in a fuel cell or in an internal-combustion-engine-driven generator—when demand exceeds production. The combustion of the H_2 to offset thermal demands has also been proposed. This renewable-energy hydrogen-storage ($RE-H_2$) concept has been studied experimentally by a number of researchers: Haas et al. (1991); Voss et al. (1996); Galli and Stefanoni (1997); Lehman et al. (1997); Barthels et al. (1998); Vanhanen et al. (1998); Hollmuller et al (2000); Agbossou et al. (2004); Hedström et al. (2004); Shakya et al. (2005); Miland (2005). The $RE-H_2$ concept has also been examined through simulation: Vanhanen and Lund (1995); Ulleberg (1998); Kolhe et al. (2003); Santarelli and Macagno (2004).

This paper represents a contribution to the $RE-H_2$ field through the use of simulation to examine the feasibility of the concept for residential buildings. A number of previous researchers have highlighted the difficulty in studying the $RE-H_2$ concept due to a paucity of performance characteristic data for key system components (e.g. Bernier et al. 2005). In both the open literature and in manufacturers' published data, for example, the reference point for efficiencies—either the H_2's lower or higher heating value—is often undeclared. Furthermore, the power consumption of ancillary devices such as pumps, controls, and power conditioners is often neglected. To address this need, models that are of the appropriate resolution for use in building simulation have been developed for the key system components. These models have been incorporated into the ESP-r building simulation program and experimental work has been conducted to calibrate model inputs.

The paper first sets out to describe the topology of the $RE-H_2$ system that is the object of the study. Following this, the models for the key system components are described. The experimental programme that was conducted to calibrate the electrolyzer and PEMFC models is then outlined. The paper concludes by presenting

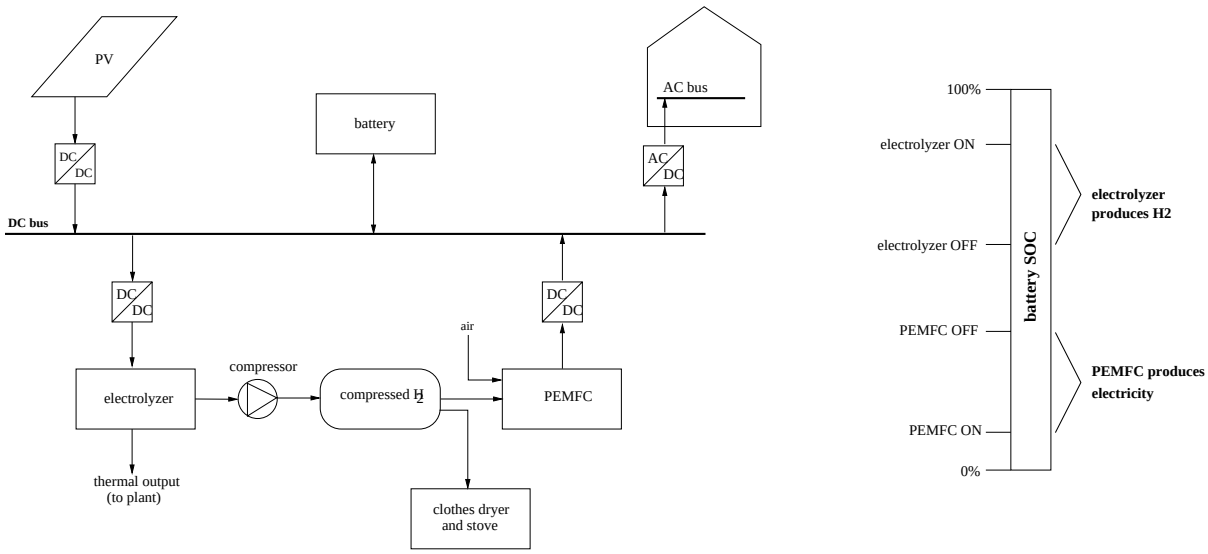

Figure 1: $RE - H_2$ **system topology (left) and system control strategy (right)**

some preliminary simulation results and outlines ongoing simulation work to assess the GHG and energy impact and the technical and economic feasibility on the concept for residential buildings.

SYSTEM TOPOLOGY

The $RE - H_2$ system that is studied in this paper is illustrated in Figure 1. The backbone of the system is a DC bus onto which flows the power produced by the PV modules and which supplies the house's power requirements through a DC-AC power inverter. A lead-acid battery regulates the voltage of the DC bus while DC-DC voltage converters allow power to flow from the DC bus to the electrolyzer and from the PEMFC to the DC bus. The H_2 produced by the electrolyzer is compressed and stored in pressurized vessels. This compressed H_2 can either be drawn off to produce electricity in the PEMFC or can be combusted for cooking and clothes drying.

The battery and H_2 path (i.e. the components appearing below the DC bus in Figure 1) are used, respectively, for short-term (up to a few days) and long-term storage. The battery has limited storage capacity but offers a high round-trip efficiency. Although the H_2 path has a much lower round-trip efficiency, it can store energy over weeks or months and can displace electricity demand for cooking and clothes drying.

This storage scheme is accomplished with a system controller whose prime input signal is the battery's normalized state of charge (SOC). The storage logic is illustrated in the right-side of Figure 1. When the battery's SOC reaches the "electrolyzer on" setpoint, excess PV production is diverted to the H_2 path. Excess PV power continues to flow to the electrolyzer until the battery is drained to the "electrolyzer off" setpoint. When the battery is drained to the "PEMFC on" setpoint the controller actuates the fuel cell to supply the house's power requirements. The deficit in PV production continues to be met by the fuel cell until the point in time that the battery is charged to the "PEMFC off" setpoint.

These and other controller setpoints are user-defined inputs. As discussed by Ulleberg (2004) these setpoints can have a significant affect upon system performance. Likewise, the capacities of system components (PV array area, battery and H_2 storage capacity, etc.), the temporal power demand pattern of the house's occupants, and weather data are strong determinants upon overall system performance.

MODEL DESCRIPTIONS

Photovoltaics

Following a review of PV models employed in building energy simulation programs (Thevenard 2005), an equivalent one-diode empirical model was selected. With this, the PV module's short-circuit current (I_{sc} in A) is calculated as follows,

$$I_{sc} = [I_{sc,ref}] \cdot \left[\frac{E}{E_{ref}}\right] \cdot \left[1 + \alpha(T_c - T_{c,ref})\right] \qquad (1)$$

Where E is the effective irradiance incident on the module (W/m^2), T_c is the cell temperature (°C), and $I_{sc,ref}$ is the short-circuit current (A) at the reference conditions of E_{ref} and $T_{c,ref}$. α is an empirical coefficient.

Similarly, the PV module's open-circuit voltage (V_{oc} in V) is calculated with,

$$V_{oc} = [V_{oc,ref}] \cdot \left[1 - \gamma(T_c - T_{c,ref})\right] \cdot max\begin{cases} 0 \\ 1 + \beta \ln\left[\frac{E_{T,eff}}{E_{ref}}\right] \end{cases} \qquad (2)$$

Where $V_{oc,ref}$ is the open-circuit voltage (V) at the

reference conditions of E_{ref} and $T_{c,ref}$ and β and γ are empirical coefficients.

When the PV module operates at its maximum power point, the produced power is given by,

$$P_{PV} = [I_{mp,ref}] \cdot [V_{mp,ref}] \cdot \left[\frac{I_{sc} \cdot V_{oc}}{I_{sc,ref} \cdot V_{oc,ref}} \right] \quad (3)$$

Where $I_{mp,ref}$ and $V_{mp,ref}$ are the current (A) and voltage (V) at the maximum power point at the reference conditions of E_{ref} and $T_{c,ref}$.

The reference conditions ($I_{sc,ref}$, $V_{oc,ref}$, $T_{c,ref}$), reference parameters ($I_{mp,ref}$, $V_{mp,ref}$) and empirical constants (α, β, γ) required by equations 1 through 3 are available in manufacturers' specifications.

In ESP-r, the PV module is represented as a multi-layered construction consisting of several material layers and each layer is represented by one or more nodes. One of these nodes represents the location of the PV cells within the module. The cell temperature (T_c) required by equations 1 and 2 is determined by solving energy balances for each node that consider the solar irradiance, convective and radiative heat transfer from the internal and external surfaces, conduction through the module, and electrical power production.

Electrolyzer

A number of electrolyzer models are available in the literature (e.g. Ulleberg 2003; Hug et al. 1993; Vanhanen and Lund 1995; Busquet et al. 2004). Most of these use empirical coefficients to describe the current-voltage relationship for the electrochemical reactions occurring at the electrolyzer stack. In some cases the power draws of ancillary equipment are ignored. In contrast, the model employed in this study considers the performance of the coherent unit. Empirical relationships are used to characterize the water consumption, auxiliary power requirements, efficiency of converting electrical power at the stack to H_2, and the oxygen production.

A single control volume is drawn to encompass the electrolyzer stack and the auxiliary equipment such as controls, gas handling equipment and a water treatment unit. (Additional control volumes representing the heat exchanger that transfers heat to an external cooling loop and a heater to temper incoming water are not treated here due to space limitations.) The energy balance representing this control volume is given as,

$$P_{stack} + P_{aux} + \dot{m}_{H_2O} h_{H_2O} + q_{gen} = \quad (4)$$

$$q_{loss} + q_{cool} + \dot{m}_{H_2} h_{H_2} + \dot{m}_{O_2} h_{O_2}$$

Where P_{stack} is the electrical power consumed by the electrolyzer stack and P_{aux} is the power draw of the auxiliary equipment. $\dot{m}_{H_2O} h_{H_2O}$ represents the enthalpy flow rate of the liquid water supply. Similarly, $\dot{m}_{H_2} h_{H_2}$ and $\dot{m}_{O_2} h_{O_2}$ represent the enthalpy flow rates of the gaseous H_2 and oxygen produced by the unit. q_{gen} is the heat generated within the control volume. q_{loss} is the heat loss from the control volume to the ambient through convection and radiation. q_{cool} is the heat transferred to the external cooling circuit. All terms in equation 4 have units of W.

A number of terms in equation 4 are expressed as empirical functions of the power supplied to the stack. This is illustrated by focusing on the H_2 production term. Firstly, the electrical conversion efficiency is defined by,

$$\eta_{el} = \frac{\dot{m}_{H_2} \cdot HHV_{H_2}}{P_{stack}} \quad (5)$$

Where HHV_{H_2} is the higher heating value of the H_2 (J/kg). An empirical function is used to express this efficiency as a function of the power supply and the electrolyzer's temperature (T),

$$\eta_{el} = e_0 + e_1 P_{stack} + e_2 P_{stack}^2 + e_3 T + e_4 T^2 + e_5 (t - t_0) \quad (6)$$

Where the e_i coefficients are derived from empirical measurements. (The topic of model calibration is treated in a subsequent section.) The last term in equation 6 represents the degradation of performance with operational time.

Equations 5 and 6 are solved at each time-step to determine the production rate of H_2 and thus the $\dot{m}_{H_2} h_{H_2}$ term of equation 4. Similar methods are used to resolve the other terms of this energy balance on a time-step basis.

Hydrogen compression

The H_2 compression device is presently modelled as a single-stage isentropic compressor. The power required by the compressor (P_{comp}) is given by,

$$P_{comp} = \frac{\dot{m}_{H_2} \cdot (h_{o,s} - h_i)}{\eta_s \cdot \eta_{motor}} \quad (7)$$

Where $\dot{m}_{H_2}$ is the flow rate of H_2 entering the compressor. h_i is the enthalpy of the gas at the inlet of the compressor and $h_{o,s}$ is the enthalpy of the gas at the outlet of the compressor if ideal isentropic compression would occur. η_s is the compressor's isentropic efficiency and η_{motor} is the efficiency of the electric motor driving the compressor.

Hydrogen storage

The compressed H_2 storage models described in the literature vary from simple state-of-charge models (eg. Miland 2005) to more complex treatments applying the ideal gas or van der Waal's state equations (eg. Ulleberg 1998). In the present study, the H_2 storage cylinders are modelled using a single control volume. The mass and energy balances in this control volume are given by,

$$\frac{dm_{cyl}}{dt} = \dot{m}_{H_2,i} - \dot{m}_{H_2,o} \quad (8)$$

$$(mC)_{cyl} \frac{dT_{cyl}}{dt} = \dot{m}_{H_2,i} \cdot (u + Pv)_{H_2,i} \quad (9)$$

$$-\dot{m}_{H_2,o} \cdot (u + Pv)_{H_2,o} - q_{loss}$$

Where m_{cyl} is the mass of the cylinder (including the encapsulated H_2), and $\dot{m}_{H_2,i}$ and $\dot{m}_{H_2,o}$ are the inlet and outlet flow rates of H_2. The variable C_{cyl} describes the combined specific heat of the cylinder wall and encapsulated H_2, while T_{cyl} describes the mass-averaged temperature of the cylinder and encapsulated H_2. The expressions $(u+Pv)_{H_2,i}$ and $(u+Pv)_{H_2,o}$ describe the specific enthalpies of the H_2 entering and exiting the cylinder, respectively. Because the outgoing H_2 exits the cylinder at the same temperature of the encapsulated H_2, the internal energy change of the H_2 exiting the cylinder will be zero, and the specific enthalpy of the outgoing H_2 reduces to $(Pv)_{H_2,o}$. Finally, q_{loss} describes the heat transfer between the cylinder and the surroundings due to convection and radiation.

PEMFC

A number of system-level PEMFC models are available in the literature (e.g. Ulleberg 1998; Amphlett et al. 1996). However, many of these focus upon the electrochemical reactions occurring within the stack and neglect the power draws of ancillary devices such as pumps, fans, and controls. In contrast, the lumped-parameter model employed in this study has been designed to facilitate calibration and considers the performance of the coherent unit. Empirical correlations characterize the unit's steady-state electrical and thermal output in response to H_2 consumption, cooling water temperature and flow rate, and performance degradation associated with prolonged use of the unit.

The heat and power produced by the PEMFC stack are calculated as fractions of the heating value of the supplied H_2, which is given by,

$$q_{HHV} = \dot{m}_{H_2} \cdot HHV_{H_2} \tag{10}$$

The stack's gross electrical output is given by,

$$P_{gross} = \eta_e \cdot q_{HHV} \tag{11}$$

Where η_e is the stack's electrical conversion efficiency. Similarly, the stack's thermal output is given by,

$$q_{recovery} = \eta_q \cdot q_{HHV} \tag{12}$$

Where η_q is the stack's thermal efficiency.

The PEMFC stack's electrical efficiency is given by:

$$\eta_e = a_0 + a_1 q_{HHV} + a_2 q_{HHV}^2 + a_3 \dot{m}_{cw} + a_4 \dot{m}_{cw}^2 \tag{13}$$

$$+ a_5 T_{cw} + a_6 T_{cw}^2 + a_7 (t - t_0)$$

Where $\dot{m}_{cw}$ (kg/s) and T_{cw} (^oC) are the flow rate and temperature of the cooling water supplied to the unit, respectively. The a_i coefficients are derived from empirical measurements. (The topic of model calibration is treated in a subsequent section.) The last term in equation 13 represents the degradation of performance with operational time.

Similar relationships are used to calculate η_q for equation 12 and the power draws of ancillaries.

Hydrogen appliances

The combustion of H_2 for cooking and clothes drying offers an efficiency advantage: approximately twice as much of the H_2's energy could be utilized compared with first converting the H_2 to electricity in the PEMFC and then powering the appliances with the electricity. Typical usage profiles were created for cooking and clothes drying. During the simulation these data along with the efficiency of the devices are used to establish the H_2 draws of the appliances as a function of time. Another input to the simulation is an electrical usage pattern for lighting and appliances. This electrical demand is reduced by a commensurate amount to account for the electrical demand that is displaced by the combustion appliances.

Power conditioning

The TRNSYS TYPE 75 model used by Ulleberg (1998) is employed for treating the DC-DC voltage converter and DC-AC inverter power conditioning units (PCU) illustrated in Figure 1. It uses an empirical relationship between the input and output power,

$$P_{in} = P_{idle} + \left(1 + \frac{V_s}{V_{out}}\right) \cdot P_{out} + \frac{R_i}{V_{out}^2} \cdot P_{out}^2 \tag{14}$$

Where P_{in} and P_{out} are the power flowing into and out of the PCU (W). P_{idle} is the power loss when the PCU is idling with a voltage over it. V_s is the setpoint voltage and V_{out} is the output voltage (V). And R_i is the PCU's internal resistance (ohms).

P_{idle}, V_s, and R_i are empirical constants that are input to the model. V_{out} results from the solution of the network represented by Figure 1. Either P_{in} or P_{out} is established for a given PCU (e.g. P_{in} is calculated by the PV model for the DC-DC converter connecting the PV module to the DC bus) while the other variable is solved using equation 14.

Battery storage

An internal-resistance model is used to represent the lead-acid battery illustrated in Figure 1. The battery's storage capacity for a given time-step is determined as a function of its temperature,

$$Q_{\max}^t = a + b \cdot T + c \cdot T^2 \tag{15}$$

Where $Q_{\max}^t$ is the maximum storage capacity (J) and a, b, and c are empirical coefficients.

The battery's normalized SOC is defined as a ratio of the energy currently stored to the maximum storage capacity,

$$SOC = \frac{Q^t}{Q_{\max}^t} \tag{16}$$

Where Q^t is the energy stored at the given time (J).

The battery's open-circuit voltage (E_0 in V) is given as an empirical function of SOC,

$$E_0 = m \cdot SOC + p \quad (17)$$

Where m and p are empirical constants.

The voltage across the battery's terminals and the current flowing from the battery to the DC bus are related as follows,

$$V = E_0 - IR_i \quad (18)$$

Where V is the voltage (V), I is the current (A), and R_i is the battery's internal resistance (ohms), which is treated as a constant user-supplied value.

The power flowing from the battery to the DC bus ($P_{battery}$ in W) is given as,

$$P_{battery} = VI \quad (19)$$

The quadratic equation formed by combining equations 18 and 19 is solved to yield the current flowing from the battery to the DC bus,

$$I = \frac{E_0 - \sqrt{E_0^2 - 4R_iP}}{2R_i} \quad (20)$$

When the battery is called upon to store or supply a given power flow, equations 15, 16, 17, and 20 are solved to determine the current flowing from the battery (charging is taken to be a negative current). Equation 18 then establishes the battery's voltage and this governs the voltage of the DC bus in Figure 1. The operation of the battery is constrained by maximum charge and discharge rates, which are in turn functions of the state of charge and temperature. The model does not yet consider self-discharging and aging effects.

MODEL CALIBRATION

A manufacturer of electrolyzer and PEMFC devices, Hydrogenics Corporation, was commissioned to conduct a series of tests to calibrate the electrolyzer and PEMFC models that were described in the previous section. The objects of these tests were Hydrogenics' 5 kW air-cooled PEM electrolyzer and its 12 kW water-cooled PEMFC.

The electrolyzer and PEMFC were subjected to four tests designed to characterize their steady-state and dynamic performance. To explore their sensitivity to operating point, the devices were modulated between zero and 100% output in increments of 10%. Sufficient time was allowed between each operating point to allow the devices to reach steady-state. Dynamic behavior was characterized in a step test modulating the device's output from 50% to 100%. Finally, measurements were taken during a cold start and a shutdown. An additional test was performed on the PEMFC to characterize its sensitivity to cooling water temperature. The unit was configured to operate at 100% output, and the cooling water inlet temperature was modulated from 35°C to 55°C in increments of 5°C.

During these tests measurements were taken on the flow rate of H_2, voltages, power flows, and (in the case of the PEMFC) the flow rate and temperature of the cooling water at the stack inlet and outlet.

Subsets of data characterizing steady-state performance were extracted from the experiments. These data were grouped according to the operating points they described, and averaged to obtain a single datum for each operating point. A least-squares regression of these averages were then performed to establish the empirical coefficients describing the performance of the electrolyzer and PEMFC (e.g. the e_i coefficients of equation 6 and the a_i coefficients of equation 13). Figure 2 illustrates the regressed form of equation 13 and demonstrates the ability of the regression to represent the measured data. (Only the first two terms of equation 13 were considered in this regression.)

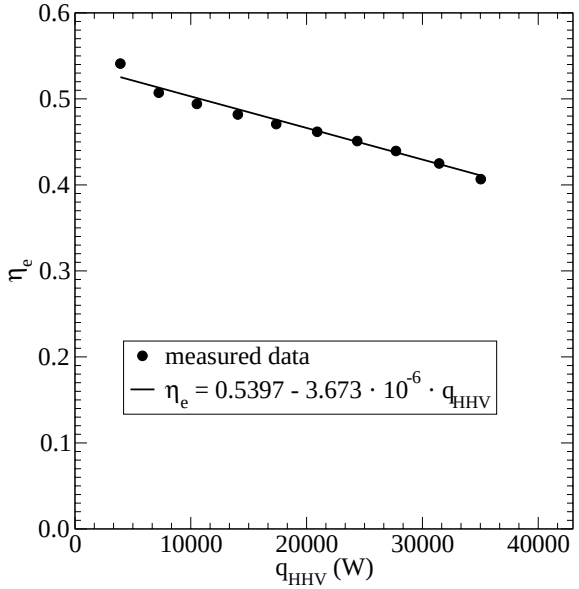

Figure 2: Calibration of equation 13

PRELIMINARY RESULTS

A simulation using Ottawa (Canada) weather data was conducted to demonstrate the new modelling capabilities. The previously described models were assembled to represent the system depicted in Figure 1. Some of the key model inputs are listed in the following table.

Figure 3 illustrates the system's operation for a typical summer day. The PV module produces more electrical energy than is demanded over the course of the day. The operation of the system is revealed by examining the trends over the day. As the PV modules produce no power until sunrise, the electrical demand is met during the early morning by drawing power from the battery (the open circles appearing below the line bisecting the

PV peak power	6.3 kW
Peak DC input to electrolyzer	4.6 kW
PEMFC peak DC output	3.5 kW
battery storage capacity	14 kWh
maximum H_2 storage pressure	12 MPa
H_2 storage volume	5 m^3
electrolyzer on setpoint	95% SOC
PEMFC on setpoint	30% SOC
average daily electricity demand	10 kWh

origin of the y-axis). From sunrise until about 9h30 the PV production exceeds the power demand and the surplus power is used to charge the battery (the open circles appearing above the line). At this point in time the battery's SOC reaches the "electrolyzer on" setpoint (refer to the earlier discussion in the *system topology* section) and the surplus power is diverted to the electrolyzer (the black circles). The system continues to produce H_2 until about 17h30, at which time the demand exceeds the PV production. Then for the rest of the day power is drawn from the batteries to supply the demand.

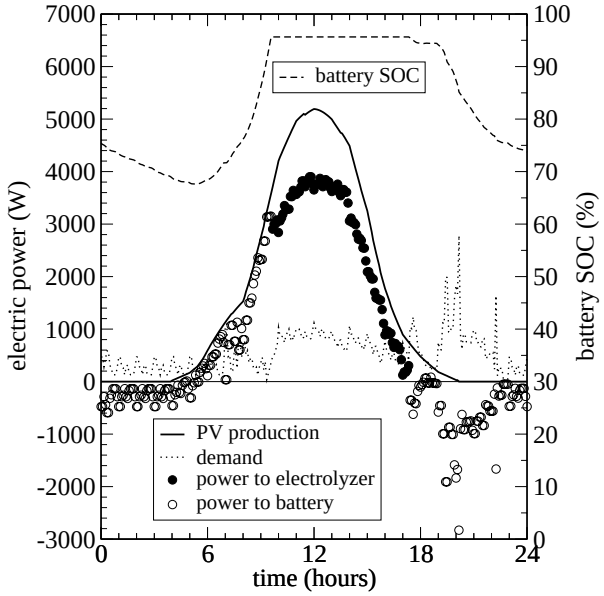

Figure 3: Typical summer day

Figure 4 illustrates the system's operation for a typical winter day. The PV module produces less electrical energy than is demanded over the course of the day. Consequently, the battery does not contain sufficient energy to meet the demand during the early morning. Rather, the PEMFC draws H_2 from the storage (which was charged earlier in the year) to supply the load. The PV module's modest electrical production from 7h45 to 8h30 is supplemented by the PEMFC to meet the demand. Once the solar radiation increases to the point where the PV module's production exceeds demand, the PEMFC is switched off and the surplus power is directed to the battery. And later in the day when the PV production drops, the energy is drawn from the battery to meet the demand. Once the battery's SOC reaches the "PEMFC on" setpoint (around 21h00) H_2 is drawn once again to supply the demand.

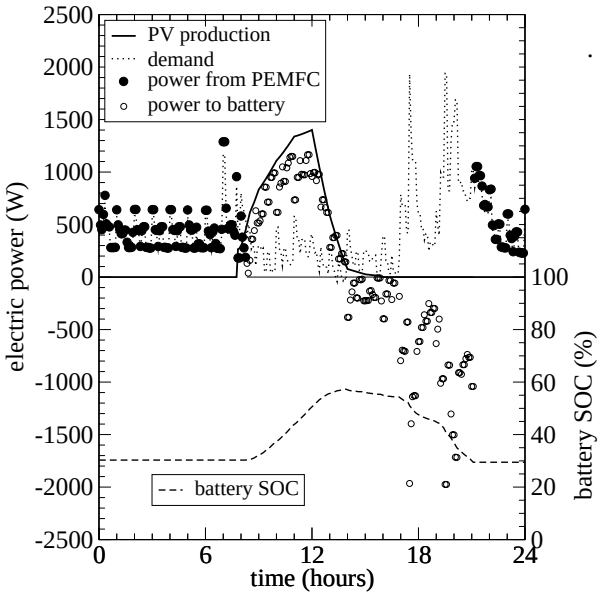

Figure 4: Typical winter day

The annually integrated electricity and H_2 flows for this simulation are displayed in Figure 5. The PV production, electrolyzer electrical consumption and H_2 production, PEMFC H_2 consumption and electrical production, H_2 combustion, and net grid import/export are presented. The figure also includes data on the ancillary power draws, PCU losses, as well as the energy flow into and out of the battery.

About one quarter of the PV module's annual electricity production of 30 GJ coincides with loads, and as such passes directly along the DC bus and through the DC-AC inverter to supply the house's lights, appliance, and the $RE - H_2$ system's ancillaries. Another quarter is diverted to the battery for short-term storage while half of the PV-produced energy follows the H_2 path.

Almost 70 kg of H_2 are produced by the electrolyzer over the year. This has an energy content of 9.9 GJ (HHV basis). More than a quarter of this H_2 is combusted for cooking and clothes drying while over half is converted back to electricity in the PEMFC. The remaining 12 kg of H_2 represents a net storage over the annual simulation, this indicating that the PV modules are oversized for the load, at least for the weather data utilized in the simulation. Net interaction with the grid over the annual simulation is seen to be negligible.

Many metrics could be calculated to assess overall system performance. For example, one could calculate the ratio of ancillary power draws and PCU losses in the H_2 path relative to power supplied to this path (27% in this

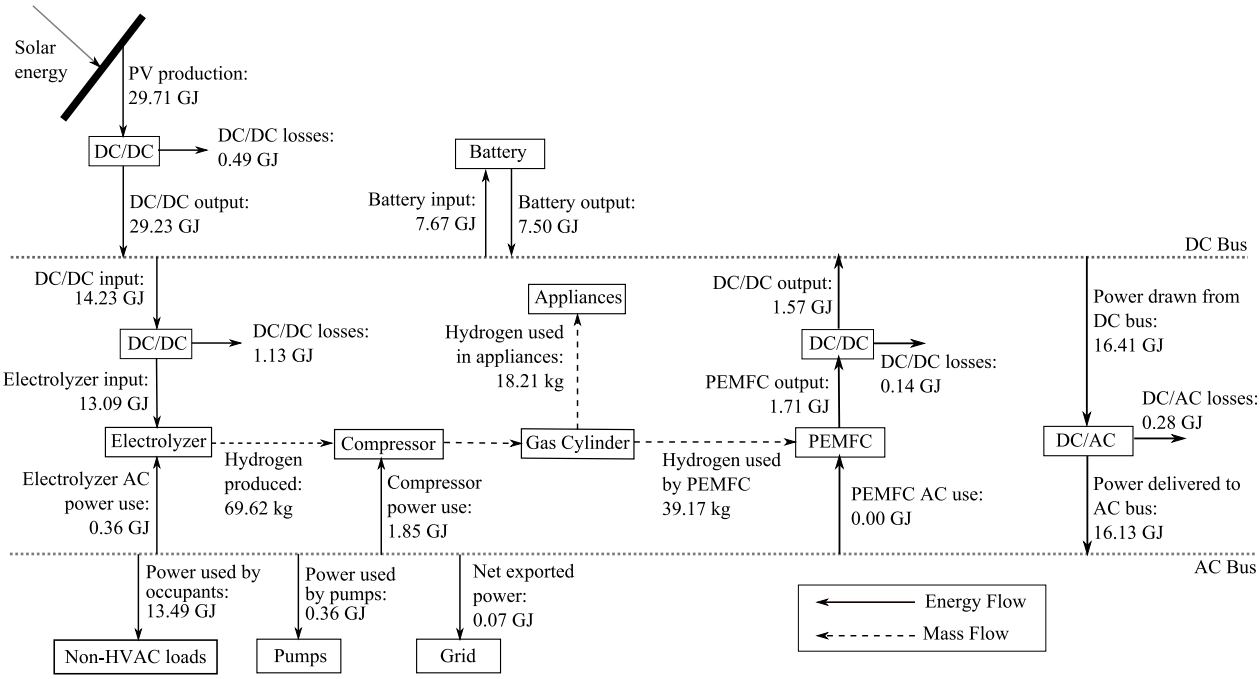

Figure 5: Annually integrated electricity and hydrogen flows

case). Another interesting metric might be the fraction of the gross PV production that serves the lighting and appliances loads (i.e. not the loads of the $RE-H_2$ system itself) and that displaces electric loads by combustion of H_2 in the appliances (52% in this case). However, for the latter one must consider that some of the energy is stored for use in future years (the 12 kg H_2 previously mentioned). The round-trip efficiency for the electricity-to-electricity route of the H_2 path can be calculated by considering the power draws of ancillaries, inefficiencies in the electrolyzer and PEMFC, and PCU losses (a low 13% in this case due to the fact that the system has not yet been optimized). However, perhaps the most interesting measure of overall system performance relates to the displaced GHG emissions. These could be calculated by considering, on a time-step basis, the emissions from the marginal source of power on the central grid that would be displaced by reducing (or eliminating) dependence upon imported power.

It is worth underlying that the results presented here are for the purpose of demonstrating the new modelling capabilities. The system studied cannot be considered optimized. Ongoing work is examining the performance of the $RE-H_2$ concept for various climate zones for numerous combinations of system component capacities, control setpoints, and occupant electricity demand profiles. This work will be based upon simulations that span multiple years using actual rather than representative weather files, so that the impact of normal annual climate variations can be considered.

CONCLUSIONS

This paper has briefly described the models that have been created within ESP-r to simulate the performance of a renewable-energy-powered electricity generation system for residential buildings. Hydrogen production, compression, and storage are key components in the system which is designed to buffer, on a seasonal basis, between electricity production and demand. The stored hydrogen can either be converted back to electricity or combusted in appliances to displace electricity demand.

The electrolyzer and PEMFC models are empirical in nature and consider the coherent systems, in that the power draws of ancillary devices are considered. The experiments that were conducted to calibrate the model inputs were briefly described. These models do not consider dynamic effects. However, the experimental data suggest that this introduces little uncertainly in assessing the overall performance of the $RE-H_2$ system. Notwithstanding, future work will study the impact of high-frequency variations upon long-term system performance in more detail. Additionally, the extension of the models and their further calibration to enable the study of cogeneration systems (i.e. heat recovery from the electrolyzer and PEMFC to displace space or water heating demand) is also planned for the future. A future paper is planned to describe the electrolyzer and PEMFC models in greater detail and to present the experimental programme that was conducted to calibrate them.

This paper demonstrated the operation of the models by simulating the performance of the $RE-H_2$ system over one year. Although this demonstrates the operation of

the models, the results must be considered inconclusive in terms of assessing the performance of the concept. Work is ongoing to establish appropriate component capacities and control strategies and to devise appropriate metrics for gauging system performance (e.g. displaced GHG emissions). Simulations will then be conducted with various system variants to assess the feasibility of the concept for numerous regions of Canada and occupancy types. These results will be reported in subsequent papers.

REFERENCES

Agbossou K., Kolhe M.L., Hamelin J., Bernier É, and Bose T.K. (2004), "Electrolytic Hydrogen Based Renewable Energy System with Oxygen Recovery and Re-Utilization", *Renewable Energy* (29) 1305-1318.

Amphlett J., Mann R., Peppley B., Roberge, P., and Rodrigeues, A. (1996) ‘‘A model predicting transient responses of porton exchange membrane fuel cells’’, *Journal of Power Sources* 61, 183-188.

Barthels H., Brocke W.A., Bonhoff K., Groehn H.G., Heuts G., Lennartz M., Mai H., Mergel J., Schmid L., and Ritzenhoff P. (1998), "PHOEBUS—Jülich: An Autonomous Energy Supply System Comprising Photovoltaics, Electrolytic Hydrogen, Fuel Cell", *Int J Hydrogen Energy* 23 (4) 295-301.

Bernier E., Hamelin J., Agbossou K., and Bose T.K. (2005), "Electric Round-Trip Efficiency of Hydrogen and Oxygen-Based Energy Storage", *Int J Hydrogen Energy* (30) 105-111.

Busquet S., Hubert C.E., Labbe J., Mayer D., and Metkemeijer R. (2004), "A New Approach to Empirical Modelling of a Fuel Cell, an Electrolyser or a Regenerative Fuel Cell", *Journal of Power Sources* (134) 41-48.

Galli S. and Stefanoni M. (1997), "Development of a Solar-Hydrogen Cycle in Italy", *Int J Hydrogen Energy* 22 5 (453-458).

Haas A., Luther J., Trieb F. (1991), "Hydrogen Energy Storage for an Autonomous Renewable Energy System—Analysis of Experimental Results", *Proc Solar World Congress*, Int Solar Energy Society, Denver USA, 723.729

Hedström L., Wallmark C., Alvfors P., Rissanen M., Stridh B., and Ekman J. (2004), "Description and Modelling of the Solar-Hydrogen-Biogas-Fuel Cell System in GlashusEtt", *J Power Sources* (131) 340-350.

Hollmuller P., Joubert J.-M., Lachal B., Yvon K. (2000), "Evaluation of a 5 kWp Photovoltaic Hydrogen Production and Storage Installation for a Residential Home in Switzerland", *Int J Hydrogen Energy* (25) 97-109.

Hug W., Bussman H., and Brinner A. (1993), "Intermittent Operation and Operation Modeling of an Alkaline Electrolyser", *Int J Hydrogen Energy* (18) 973-977.

Kolhe M., Agbossou K., Hamelin J., Bose T.K. (2003), "Analytical Model for Predicting the Performance of Photovoltaic Array Coupled with a Wind Turbine in a Stand-Alone Renewable Energy System Based on Hydrogen", *Renewable Energy* (28) 727-742.

Lehman P.A., Chamberlin C.E., Pauletto G., and Rocheleau M.A. (1997), "Operating Experience with a Photovoltaic-Hydrogen Energy System", *Int J Hydrogen Energy* 22 5 (465-470).

Miland H. (2005), *Operational Experience and Control Strategies for a Stand-Alone Power System based on Renewable Energy and Hydrogen*, Ph.D. Thesis, Norwegian University of Science and Technology, Trondheim Norway.

Santarelli M. and Macagno S. (2004), "A Thermoeconomic Analysis of a PV-Hydrogen System Feeding the Energy Requests of a Residential Building in and Isolated Valley in the Alps", *Energy Conversion and Management* 45 (427-451).

Shakya B.D., Aye L., and Musgrave P. (2005), "Technical Feasibility and Financial Analysis of Hybrid Wind-Photovoltaic System with Hydrogen Storage for Cooma", *Int J Hydrogen Energy* (30) 9-20.

Thevenard D. (2005), "Review and Recommendations for Improving the Modelling of Building Integrated Photovoltaic Systems", *Proceedings of Building Simulation 2005* (1221 - 1228).

Ulleberg Ø (1998), *Stand-Alone Power Systems for the Future : Optimal Design, Operation, and Control of Solar-Hydrogen Energy Systems*, Ph.D. Thesis, Norwegian University of Science and Technology, Trondheim Norway.

Ulleberg Ø (2003), "Modeling of advanced alkaline electrolysers: a system simulation approach", *nt J Hydrogen Energy* (28) 21-33.

Ulleberg Ø (2004), "The Importance of Control Strategies in PV-Hydrogen Systems", *Solar Energy* (76) 323-329.

Vanhanen J.P. and Lund P.D. (1995), "Computational Approaches for Improving Seasonal Storage Systems Based on Hydrogen Technologies", *Int. J. Hydrogen Energy* 20 (7) 575-585.

Vanhanen J.P., Lund P.D., and Tolonen J.S. (1998), "Electrolyser-Metal Hydride-Fuel Cell System for Seasonal Energy Storage", *Int J Hydrogen Energy* 23 (4) 267-271.

Voss K., Goetzberger A., Bopp G., Häberle A., Heinzel A., and Lehmberg H. (1996), "The Self-Sufficient Solar House in Freiburg—Results of Three Years of Operation", *Solar Energy* 58 (17-23).